J. Ind. Geophys. Union, 28(6) (2024), 439-448

Identification of potential iron ore zones in parts of Singrauli District, Madhya Pradesh using ASTER sensor data

Koppu Thirupathi and Ram Raj Mathur
Centre of Exploration Geophysics, Department of Geophysics, Osmania University, Hyderabad-500007, Telangana, India
Corresponding author: kopputhirupathi@osmania.ac.in

ABSTRACT

The remote-sensing approach offers a chance to enhance the first stages of mineral discovery by detecting and mapping surface minerals. The reflectance spectra of various minerals in the visible-near infrared (VNIR) region are primarily influenced by the presence or absence of transition metal ions such as Fe, Cr, Co, and Ni. The discovery of these objects is made possible by their distinctive spectral signatures. This paper aims to analyse remote sensing data obtained from the ASTER sensor, in order to identify possible areas rich in iron ore. The data was obtained from the USGS Earth Explorer. The analysis was conducted using the ENVI 5.0 software. The processing sequence consists of series of operations performed on obtained data set. Broadly, these include the false colour composite image enhancement, image contrast, different filters and band ratio techniques, etc. Using these techniques, the present study reveals a north-northwest (NNW) section of the study area to have deposits of banded iron formation (BIF). Analysing ASTER data independently using their sensor-resampled laboratory spectra of BIF, allows for the identification of surface anomalies of Fe- enrichment.

Keywords: Iron ore zones, Remote sensing, ASTER Data, Radiometric correction, Band ratio techniques

INTRODUCTION

The remote-sensing technique provides an opportunity to improve understanding of the geological structures and indicators for mineral exploration by identifying the spectral signatures (Moghtaderi et al., 2007; Zhang et al., 2007; Gabr et al., 2010; Raj et al., 2015; Ducart et al., 2016). Many researchers have used satellite data to detect various minerals present in the earth's surface through image enhancement technique, Principal Component Analysis (PCA), spectral analysis and Band Ratio techniques (Gabr et al., 2010; Pour and Hashim, 2012).

The launch of the Japanese ASTER sensor on board the US Terra satellite in December 1999, signaled the start of a new era in mapping the earth's surface composition. Although Landsat satellite Thematic Mapper (TM) data has proved useful for regional geological studies, its coarse spectral resolution precludes detailed mapping of geological composition. It has been shown by several investigators at various test sites that the multi-spectral visible-shortwave remote sensing can successfully map areas of prospective geological alteration and key mineral groups (Hewson et al., 2001). The presence or lack of transition metal ions (e.g. Fe, Cr, Co, Ni) in different minerals, dominate their reflectance spectra in the visible-near infrared (VNIR) and near infrared (NIR), regions leading to absorption characteristics caused by electronic processes (Van Deer Meer and De Jong, 2012). Iron oxide minerals, such as jarosite, haematite, and limonite, exhibit spectral absorption characteristics in the visible to medium infrared range of the electromagnetic spectrum ranging from 400 to 1100 nm (Hunt and Ashley, 1979). Attempts on mapping of the iron-bearing formation to delineate surface distributions of iron exposures using remote sensing data, are well discussed in the literatures (Rajendran et al., 2011; Magendran and Sanjeevi, 2014; Bersi et al., 2016). In many of these studies, utilization of remote sensing data in targeting iron bearing minerals was focused on using diagnostic absorption features of iron-bearing rock formations based on their reflectance spectra.

In the present paper an attempt has been made to interpret the remote sensing data using the ASTER sensor in Singrauli district (Figure 1) of Madhya Pradesh, India to identify the potential iron ore zones. The data was acquired from the USGS Earth Explorer data and downloaded from their website. The analysis was carried out by using ENVI 5.0 (Environment for Visualizing Images) software.

GEOLOGY OF THE STUDY AREA

The present study area is located in the Singrauli district of Madhya Pradesh (Figure 1). It covers an area of approximately 63 sq. km on the Survey of India topo sheet no 63L/7. The district is bounded in the north by Rewa and Sidhi districts, in the east by Uttar Pradesh, in the south by Sarguja, and on the west, by Shahdol district. The Mahakoshal Group of the rocks (Table 1) on its southern margin are bounded by gneissic-granites and the Gondwana Group of rocks and on the northern side of the belt, it is in contact with the Vindhyan Supergroup. Near Sidhi, a linear belt of gneissic granite intervenes are also present.

Prominent geological structures

Horizontal bedding is the only planar non-diastrophic and non-penetrative structure indicated by the Mahakoshal rocks and is seen in the banded magnetite, banded haematite quartzite, dolomite of Agori formation and the felspathic quartzites of Parsoi Formation and is marked by compositional layering and color banding. The thickness of the stratification laminae in the BIF (banded iron formation) varies from a few mm to 5 cm. A series of ENE-WSW trending overturned isoclinal folds control the exposure pattern of the Mahakoshal Group. This group is characterized by two boundary faults known as the Son-Narmada north fault and the Son-Narmada south fault. The north fault extends uninterruptedly from the northwest of Narsinghpur in Madhya Pradesh to the northern region of Agori in Uttar Pradesh. The maximum region of this fault runs along the river course. Further east, this contact is marked by the Amsi-Kharundhi fault. Evidence of faulting in the form of silicification, brecciation, and close spaced jointing, sudden steepening and overturning of beds have been recorded along this zone.

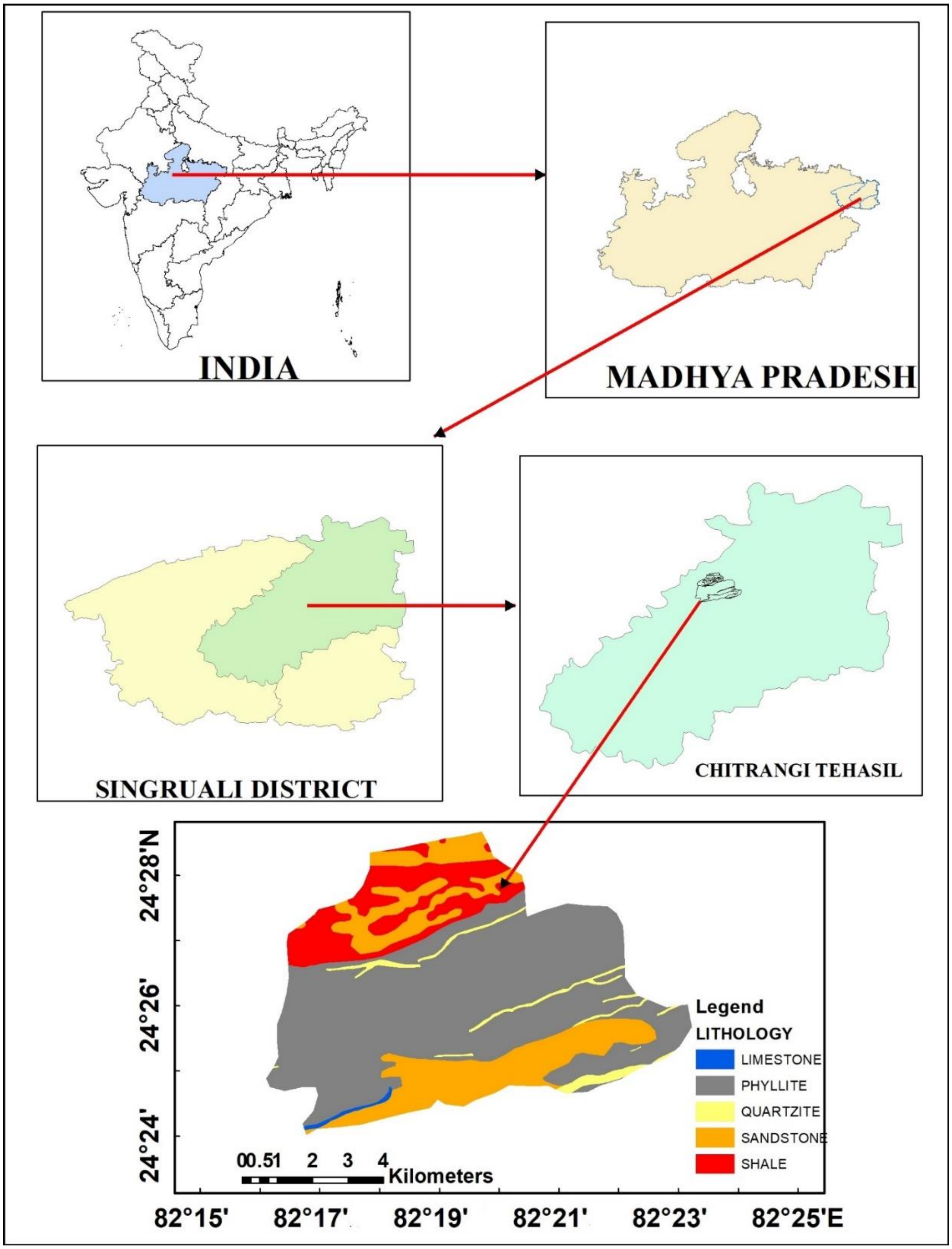

Figure 1. Map of the study area. Source: BHUKOSH, GSI (https://bhukosh.gsi.gov.in/Bhukosh/Public)

Table 1. Lithostratigraphic succession of the rocks of Singrauli area, Madhya Pradesh (modified after GSI CRUMANSONTATA project from 1978 to 1988)

Lithology	Formation	Group	Age
Vindhyan Supergroup and jungle Group of Sediment			
---------------Unconformable and faulted contact-----------------			
Dunite, gabbro dolerite, quartz-porphyry and quartz veins, syenite and associated alkaline dykes, carbonatites, barite veins and lamprophyres/trachytes and associated intrusives. Barambaba granite and equivalents	Intrusives	MAHAKOSHAL GROUP	PALAEOPROTEROZOIC
Tuffaceous and carbonaceous phyllites, feldspathic quartzite and conglomerate, tuffaceous phyllite with basalt intercalations	Parsoi Formation		
Banded haematite/magnetite quartzite and jasperoid beds with associated tuffs and ash beds. Impure marble, dolomite and interbedded calc-chlorite schist with occasional metabasalt lenses, conglomerate	Agori Formation		
Basic and ultrabasic plugs and dykes including peridotite and serpentine, Agglomerates, metabasalt and peridotite pillow lava	Chitrangi Formation		
--------Fault--------Locally Unconformable--------------------------			

METHODOLOGY

Most shallow occurring minerals have distinct spectral signatures in the visible and near-infrared (VNIR) and shortwave infrared (SWIR) regions of the electromagnetic (EM) spectrum. These spectral signature characteristics allow for the detection of enriched mineral rocks (Yitagesu et al., 2011; Vicente and de Souza Filho, 2011; Hewson et al., 2012). Hence, the present work utilizes ASTER data (Table 2) to identify the iron ore reserves and related alteration zones in the Singrauli region.

The ASTER device utilizes spectral bands in the visible and near-infrared range, spanning from 0.52 to 0.86 μm, as well as in the shortwave infrared range, spanning from 1.6 to 2.43 μm to detect and quantify the volume of reflected radiation. The instrument has a resolution of 15 and 30 m for VNIR bands and SWIR bands respectively (Fujisada, 1995). Additionally, ASTER is equipped with a rear-facing VNIR telescope that has a resolution of 15 m. Therefore, it is possible to obtain stereoscopic VNIR images with a resolution of 15 m. The radiation that is released is quantified with a precision of 90 m in five specific bands ranging in wavelength from 8.125 to 11.65 μm thermal infrared (TIR).

The ASTER standard deliverables include surface radiance and reflectance measurements in the visible and shortwave infrared (VNIR and SWIR) regions, as well as brightness temperature readings at the sensor. The measurements also include surface radiance and emissivity in the thermal infrared (TIR) region, surface kinetic temperature, decorrelation-stretch images, and digital-elevation models (DEM). The visible-near infrared, shortwave infrared, and thermal infrared wavelengths offer supplementary information that is valuable for lithologic mapping. The three visible near-infrared bands provide valuable data on the absorption properties of transition metals, particularly iron and some rare-earth elements (REE) (Rowan et al., 1986). The mineralogical mapping of this specific range of wavelengths has been widely employed by using advanced imaging methods with great spectral resolution, such as the Airborne Visible/Infrared Imaging Spectrometer (AVIRIS) (Kruse, 1988; Clark, et al., 1991; Crowley, 1993; Boardman and Kruse, 1994; Rowan et al., 1996). This paper focuses on the analysis of ASTER data obtained between April 30, 2007, and March 3, 2008, having WRS Path No 142 and WRS Row No 43 of the Terra satellite over the Singrauli district of Madhya Pradesh state. The objective is to identify and delineate areas with potential for iron ore deposits as stated earlier.

Table 2. Specification of selected bands of ASTER sensor used for this study

Satellite/Sensor	Subsystem	Band number	Spectral range (µm)	Spatial resolution (m)	Radiometric resolution
ASTER (Acquisition date) Scene1:June-1-2007, Scene2:April-30-2007, Scene3: March-3-2008)	VNIR	1	0.52-0.60	15 meter	8 bits
		2	0.63-0.69		
		3	0.78-0.80		
	SWIR	4	1.6-1.7	30 meter	
		5	2.145-2.185		
		6	2.185-2.225		
		7	2.235-2.285		
		8	2.295-2.365		
		9	2.36-2.43		

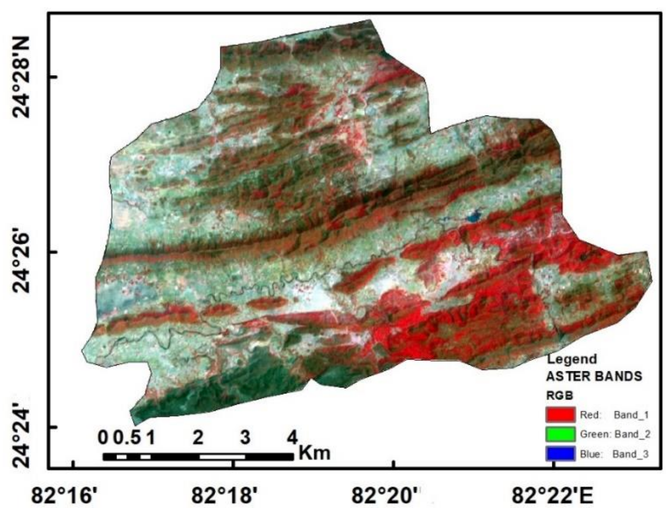

Figure 2. ASTER Image (2007). Source: USGS Earth explorer. The image contains 12 bands in which, 3 are VNIR bands, 6 SWIR bands and 3 TIR bands of 15 m, 30 m and 90 m resolution respectively

PRESENT APPROACH

The current study aims to detect the concentration of iron-rich minerals on the surface by utilizing ratio images from both sensors. In the study area, there are few exposures of iron formations, smaller than the pixel size of spectral bands of ASTER data and most of them are covered with vegetation (Figure 2).

The actual surface exposures of iron-rich rock units cannot be resolved using the per-pixel mapping method. Therefore, a match filtering method has been implemented for processing spectral bands of ASTER data in which respective sensor-resampled BIF spectra are used as a reference for processing respective images of two different sensors. Results of per pixel and sub-pixel spectral maps of ASTER data have been integrated. In view of the megascopic geomorphic signatures of different rock units, we have identified suitable geomorphic signatures of iron bearing formation.

The outline of these geomorphic land units (the folded ridge of different wavelengths), has been taken as a reference to identify a few promising areas for further exploration. Field based delineation of iron-rich rock units like Banded Iron Formation (BIF) and Banded Haematite Jasper (BHJ), can be taken as validation reference to confirm the Fe-enrichment on the surface (Figure 3). The entire methodology followed in the present study has been presented in data processing section.

DATA PROCESSING

The pre-processing stages for calibrating ASTER data include converting radiance to reflectance, creating a mosaic, and selecting a subset of the original data based on the spatial extent of the study area (Table 2). The ASTER Level-1B data processed for the present study area is shown in Figure 2. ASTER VNIR and SWIR sub-systems have nine spectral bands that are capable of targeting iron-rich minerals and are also suitable for mapping iron residue (Rajendran et al., 2011). Radiometric calibration is performed on ASTER VNIR (Figure 4), SWIR (Figure 5), and TIR (Figure 6) data to enhance the picture data for radiance, reflectance, or brightness temperatures. Image fusion in remote sensing involves merging many distinct photos using a specific algorithm to generate a novel image. The Atmospheric Correction Module (ACM) can be applied once layer stacking (Figure 7) is done to VNIR and SWIR spectral bands which are enhanced and comprehensive. The atmospheric correction applied to layer stack image as shown in Figure 8.

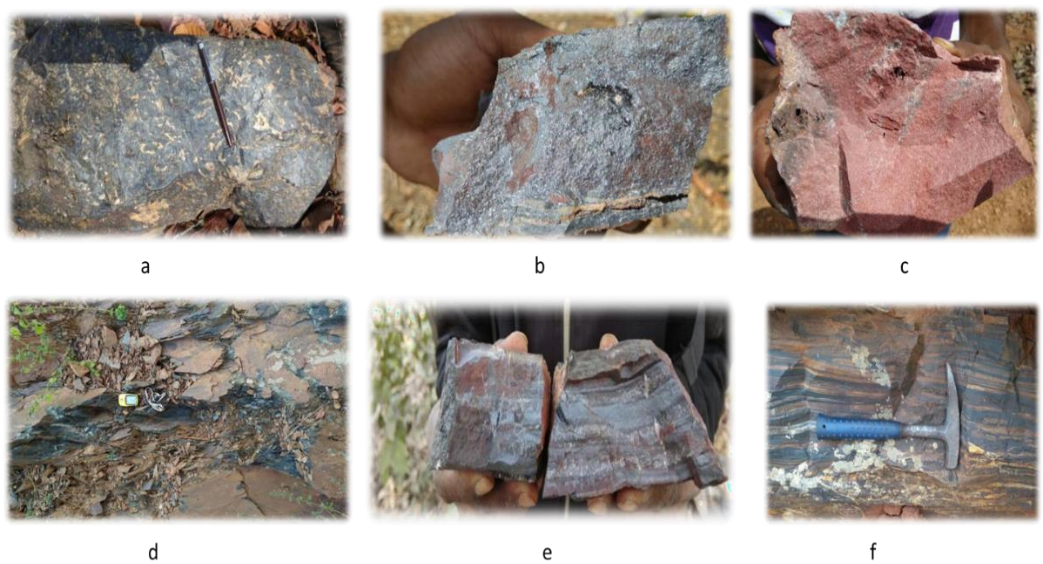

Figure 3. Different types of rock units in the study area. **(a)** Quartz veination in haematite, **(b)** Haematite- rich in micaceous minerals, **(c)** Ferrugeneous quartzite, **(d)** Grey coloured phyllite, **(e)** Banded haematite jasper and **(f)** Color banding and stratification in banded haematite jasper.

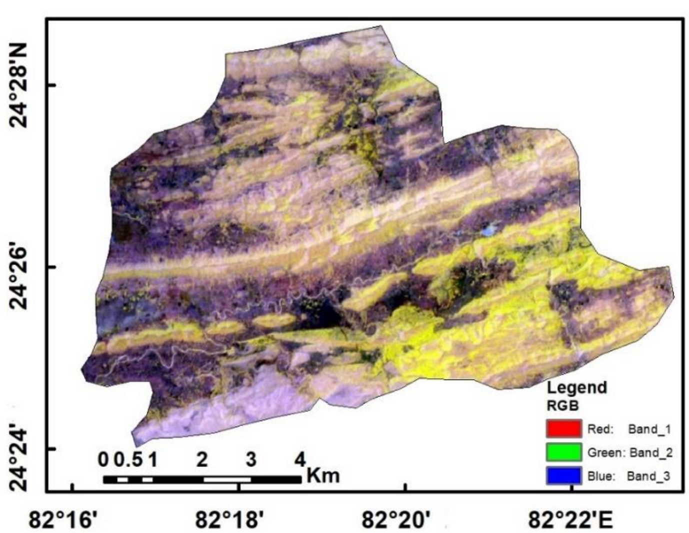

Figure 4. VNIR ASTER image after radiometric correction applied to the satellite map taken from the USGS earth Explorer

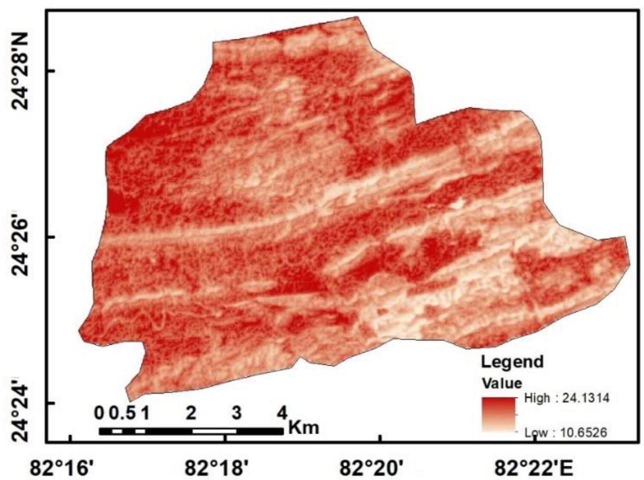

Figure 5. SWIR Aster image after radiometric correction applied to the satellite map taken from the USGS earth Explorer

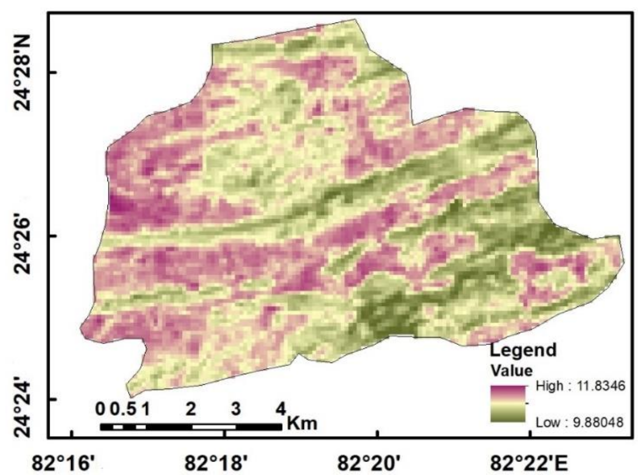

Figure 6. TIR Aster image after radiometric correction applied to the satellite map taken from the USGS earth Explorer

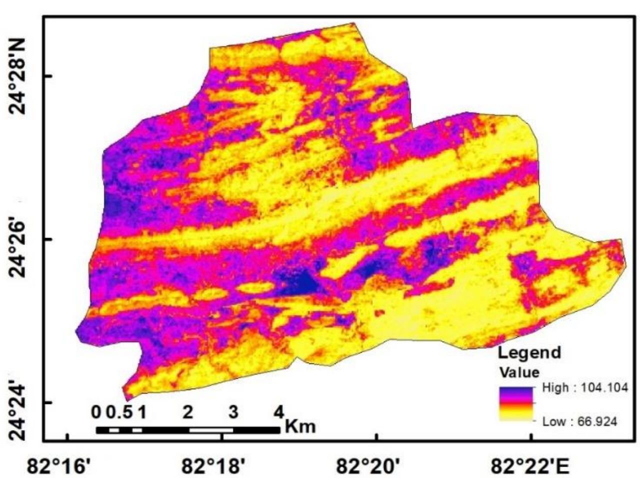

Figure 7. Stacked image of VNIR and SWIR ASTER data after applying layer stack

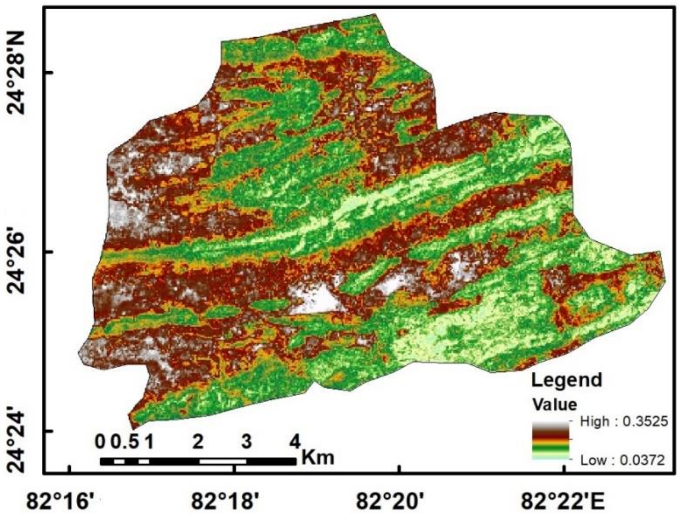

Figure 8. ASTER image after atmospheric correction applied to the layer stacked image

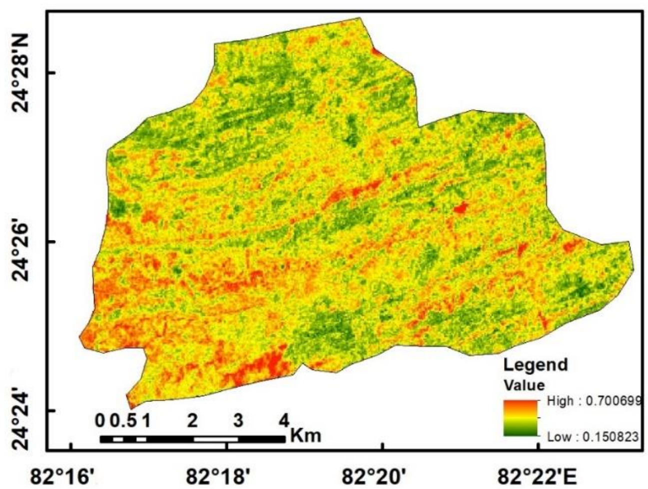

Figure 9. Map of ferrous minerals after application of Band ratio technique to the Atmospherically corrected image

Further, in recent times, the Band ratios technique is widely used to amplify the spectral distinctions between bands and mitigate the impact of topography. The image amplifies the spectral disparities among bands (Figure 9). This band ratio gives information about iron-bearing minerals (https://pro.arcgis.com/en/pro-app/latest/arcpy/image-analyst/ferrousminerals.htm; Imbroane et al., 2007)

$$Ferrous\ mineral\ ratio = \frac{SWIR}{NIR}$$

The SWIR range is from 1.55 to 1.75 µm, whereas the NIR range is from 0.76 to 0.9 µm. For Landsat TM, ASTER, and ETM+, this corresponds to spectral bands 5 (shortwave infrared) and 4 (near infrared). This index is compatible with multispectral sensors that have bands falling within the specified ranges. In addition, the utilization of principal component (PC) analysis on ASTER bands 3, 2, and 1, has demonstrated its efficacy by enhancing the identification of iron ores, resulting in a distinctive chocolate brown colour (Rajendran et al., 2011). Surface anomalies for iron occurrence exhibited significant magnitude in all of these studies, thereby necessitating the development of per-pixel mapping techniques.

The major steps involved in processing ASTER data are scaling of the reflectance bands, resampling of the spectral profiles of rocks to the bandwidth of the two sensors (ASTER VNIR-SWIR), validation of relative reflectance products, and implementation of spectral mapping methods. In the study area, rocks like ferruginous quartzite, BIF, lateritic soil, and Fe-rich phyllites are present and all of them contain Fe-oxides. Therefore, the match filtering method is applied to both the data (i.e. spectral bands of ASTER) to estimate the sub-pixel occurrence of iron ore. The band ratio image and MF image derived from ASTER data are combined using the principal component image. Above mentioned PC-1 images derived independently from each sensor are indicative of the iron enrichment. These images were derived from the results of per pixel and sub pixel spectral maps of each sensor. From these images the iron ore anomaly map of each sensor is integrated in the map by merging the spectral anomalies with other geological data sets for targeting iron ore deposits. The iron ore anomalies detected in ASTER bands are reconciled based on deriving correlation of images by integrating anomaly maps of each sensor. Integration of a merged spectral map of each sensor help in reducing the contribution of sensor parameters in spectral mapping and also help in removing non-coherent information of different standalone spectral maps. This indirectly reduces the false positives in spectral maps. Further, the spatial extent of iron-bearing BIF is used as limiting boundary iron ore enrichment, which may lead to identifying a new deposit as deposit-level iron enrichment is expected within the BIF rocks of Agori formation. Therefore, a unified spectral map has been clipped using the outline of the BIF formation of the area (Figure 9).

RESULTS

Spectral profiles of different samples of BIF and associated rocks have been analyzed (Figure 10). Spectrally, iron bearing formations are identified with prominent absorption features at 550 nm and 900 nm (Figure 9). It has been found that diagnostic absorption features Fe-quartzite, laterite, and BIF are spectrally close to each other. BIF has strong absorption around 900 nm while laterite was featureless with a small kink in this wavelength. Fe-bearing quartzite and low-grade BIF have an absorption feature at this wavelength (i.e., 900 nm) but with a lower absorption depth. Absorption features at 550 nm are common for laterite and BIF. These two features are crucial for detecting iron bearing formations. In a nutshell, electronic processes are responsible for the absorption feature of around 550 nm, while the crystal field process is responsible for the absorption feature of around 900 nm (Clark and Roush 1984; Cloutis, 1996). BIF samples are found to have their diagnostic absorption feature at lower wavelengths with respect to the wavelength of diagnostic absorption of Fe-bearing quartzites. Diagnostic features of BIF are 10-20 nm apart from the spectra of other rocks (e.g. laterite, Fe-quartzite, etc.). This has been observed by the spectrometric plot of absorption features at 850-900 nm. This contrast only can be detected using hyperspectral data having finer spectral bandwidth of 10 nm. The spectral contrast of different rocks in the study area has been further reduced when the spectra are resampled to the bandwidth of two sensors. Here, ASTER data are processed to map spectral anomalies associated with iron ore enrichment in the study area using respective sensor-resampled spectra. Independent spectral maps have been derived from the ASTER data using band ratio and matched filtering images. Band ratio images delineated BIF and associated laterite as their broadband spectra for selected bands are the same and also both band ratio derive known absorption features of iron-bearing minerals as these features were used to highlight the BIF absorption at 880 nm (in case of Landsat-8 OLI ratio using band 5 by band 4) and another BIF feature at 450-550 nm, ratio derived using band 2 and band 1 of ASTER data.

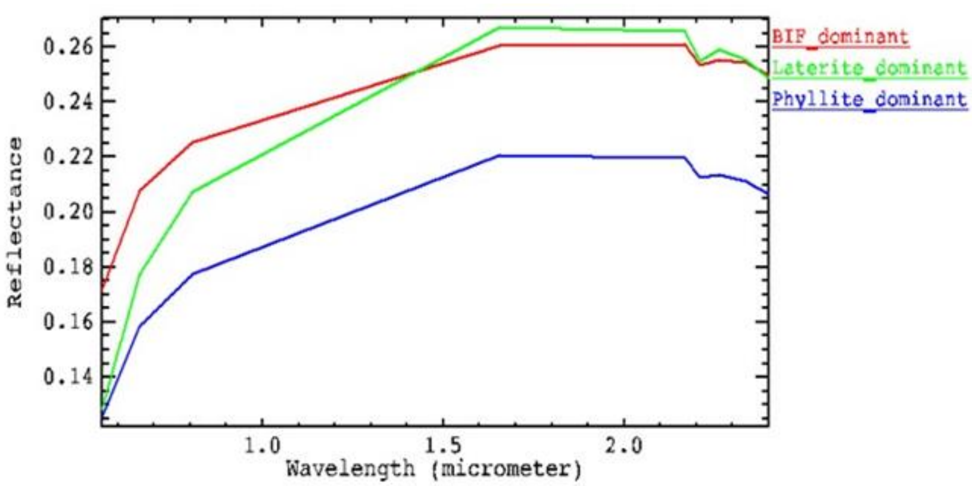

Figure 10. Mixed spectral response of different rocks. Mixed spectra are derived based on the assumption that the major litho-components are linearly mixed in ASTER data.

Ratio images are effective when a spectral feature of the target is unique concerning the spectral feature of the associated rocks and the target is well distributed on the surface. Also, two spectral anomaly maps have been integrated from two different sensors into a single map resulting in a correlated image of the spectral anomaly map of two sensors. In the study area, the Banded Iron Formation (BIF) of Agori Formation, is the main source rock of iron oxides. Therefore, the surface anomaly map of iron-enrichment has been further restricted by sub-setting the final spectral maps using the outline of BIF of Agori formation. Knowledge-based spatial sub-setting of spectral maps would help in eliminating the false positives of spectral maps.

DISCUSSION AND CONCLUSIONS

The processed ASTER data could have created several false positive and over estimation of the iron formations in the individual spectral maps due to the presence of a mixed spectrum influencing the detection of the anomalous zones. Further, the detection of iron-bearing formations from Space-borne spectra data could be hampered, if organic carbon is present on the surface, especially in the present study area of the Siddhi region. Also, most of the iron-rich zones in the study area were present under forest cover. Hence, to delineate iron-bearing exposures having exposure sizes less than the ASTER and Landsat-8 pixels, we attempted a matched filtering method. However, the accuracy of spectral anomaly maps derived based on processing sub-pixel spectral mapping methods like match filtering, is governed by the spectral contrast of target and background rocks (Shippert, 2003). Following conclusions can be drawn from the present work.

(1) This study confirmed that the NNW part of the study area (Figure 9) contains potentially rich BIF zone and thus recommended for further geophysical investigations.

(2) Independent analysis of ASTER data using their sensor-resampled spectra of BIF could delineate surface anomalies of Fe-enrichment, based on the implementation of per pixel method (Band ratio method).

(3) Poor broad-band spectral contrast of different iron-bearing rocks, the presence of forest cover, and patchy exposures of targets are the major constraints for spectral mapping.

(4) Spatial constraining of spectral maps based on the geomorphic outline of BIF bearing iron formation, are done by the integration of spectral maps of two sensors that reduces the role of sensor parameter in spectral mapping and also reduce the false positives of the spectral map.

ACKNOWLEDGMENT

We express our sincere gratitude to the Centre of Exploration Geophysics, Osmania University, Hyderabad for permitting us to conduct this investigation. Our sincere thanks to the USGS Earth Explorer for providing ASTER satellite data for this study.

Author Credit Statement

Koppu Thirupathi: Data acquisition, conceptualization, processing, interpretation and paper draft preparation. Ramraj Mathur: validation, supervision, reviewing, editing and finalization of the paper

Data Availability

The data utilized in this investigation is accessible through the USGS Earth Explorer.

Compliance with Ethical Standards

This work was carried out as a component of a doctoral programme in the Department of Geophysics, Osmania University, Hyderabad. This paper is the author's original work, which has not been previously published elsewhere. Authors adhere to copyright norms.

REFERENCES

Bersi, M., Saibi, H. and Chabou, M.C., 2016. Aerogravity and remote sensing observations of an iron deposit in Gara Djebilet, southwestern Algeria. J. Afr. Earth. Sci., 116, 134-150.

Boardman, J. W. and Kruse, F. A., 1994. Automated spectral analysis: a geologic example using AVIRIS data, north Grapevine Mountains, Ne vada. Proc. Tenth Thematic Conf. on Geol. Rem. Sens., I407–I418.

Clark, R. N. and Roush, T. L., 1984. Reflectance spectroscopy: Quantitative analysis techniques for remote sensing applications. J. Geophy. Res. Sol. Ear., 89(B7), 6329- 6340.

Clark, R. N., Swayze, G. A., Gallagher, A. J., Gorelick, N. and Kruse, F. A., 1991. Mapping with imaging spectrometer data using the complete band shape least-squares fit to multiple spectral features from multiple materials. Proc. Third AVIRIS Work. JPL Publ., vol. 91-28, pp. 2–3.

Cloutis, E. A., 1996. Review Article Hyperspectral geological remote sensing: evaluation of analytical techniques. Int. J. Rem. Sen., 17 (12), 2215-2242.

Crowley, J. K., 1993. Mapping playa evaporite minerals with AVIRIS data: a first report from Death Valley CA. Rem. Sen. Env., 44, 337–356.

Ducart, D.F., Silva, Toledo, B. and Assis, L., 2016. Mapping iron oxides with Landsat-8/OLI and EO-1/Hyperion imagery from the Serra Norte iron deposits in the Carajas Mineral Province, Brazil. Braz. J. Geol., 46 (3), 331–349.

Fujisada, H., 1995. Design and performance of ASTER instrument. Int. Soc.. for Opt. Eng., 2583, 16–25.

Gabr, S., Ghulam, A. and Kusky, T., 2010. Detecting areas of high-potential gold mineralization using ASTER data. Ore Geol. Rev., 38 (1), 59–69.

Hewson, R. D., Cudahy, T. J. and Huntington, J. F., 2001. Geologic and alteration mapping at Mt Fitton, South Australia, using ASTER satellite-borne data. Int. Geosci. and Rem. Sens. Symp., 2, 724-726.

Hewson, R.D., Cudahy, T.J., Jones, M. and Thomas, M., 2012. Investigations into soil composition and texture using infrared spectroscopy (2–14 m). Appl. and Env. Soil Sci., 1–12. doi:10.1155/2012/535646

Hunt, G.R. and Ashley, R.P., 1979. Spectra of altered rocks in the visible and near infrared. Economic Geology, 74 (7), 1613–1629.

Imbroane, M. A., Melenti, C. and Gorgan, D., 2007. Mineral explorations by Landsat image ratios. In: Ninth Int. Sym. on Symb. and Num. Algor. for Sci. Comp. *(SYNASC 2007)*, pp. 335-340.

Kruse, F. A., 1988. Use of airborne imaging spectrometer data to map minerals associated with hydrothermally altered rocks in the northern Grapevine Mountains, Nevada–California. Rem. Sens. Env., 24, 31–52.

Magendran, T. and Sanjeevi, S. 2014. Hyperion image analysis and linear spectral unmixing to evaluate the grades of iron ores in parts of Noamundi, Eastern India. Int. J. App. Ear. Obs. and Geoinf., 26, 413-426.

Moghtaderi, A., Moore, F. and Mohammadzadeh, A., 2007. The application of advanced space-borne thermal emission and reflection (ASTER) radiometer data in the detection of alteration in the Chadormalu paleocrater, Bafq region, Cent. Iran. J. Asian Earth. Sci., 30 (2), 238–252.

Pour, A.B. and Hashim, M., 2012. The application of ASTER remote sensing data to porphyry copper and epithermal gold deposits. Ore Geol. Rev., 44, 1–9. doi:10.1016/j.oregeorev.2011.09.009

Raj, S.K., Ahmed, S.A., Srivastav, S.K. and Gupta, P.K., 2015. Iron oxides mapping from E0-1 Hyperion data. J. Geol. Soc. Ind., 86 (6), 717–725.

Rajendran, S., Thirunavukkarasu, A., Balamurugan, G. and Shankar, K., 2011. Discrimination of iron ore deposits of granulite terrain of Southern Peninsular India using ASTER data. J. Asian Earth Sci., 41 (1), 99–106.

Rowan, L. C., Kingston, M. J. and Crowley, J. K., 1986. Spectral reflectance of carbonatite and related alkalic igneous rocks from four North American localities. Econ. Geol., 81, 857–871.

Rowan, L. C., Clark, R. N. and Green, R. O., 1996. Mapping minerals in the Mountain Pass, California area using Airborne Visible–Infrared Imaging Spectrometer (AVIRIS) data. Proc. 11th Conf. on Geologic Remote Sensing, vol. 1, pp. I177–I178.

Shippert, P., 2003. Introduction to hyperspectral image analysis. Online J. of Space Comm., 3.

Van Deer Meer, F. and De Jong, S.M., 2012. Multi-and hyperspectral geologic remote sensing: A review. Int. J. Appl. Earth Obs. Geoinf., 14 (1), 112–128.

Vicente, L.E. and de Souza Filho, C.R., 2011. Identification of mineral components in tropical soils using reflectance spectroscopy and advanced spaceborne thermal emission and reflection radiometer (ASTER) data. Rem. Sens. Env., 115 (8), 1824–1836.

Yitagesu, F.A., Meer, F., Werff ,H. and Hecker, C., 2011. Spectral characteristics of clay minerals in the 2.5–14μm wavelength region. Applied Clay Sci., 53 (4), 581–591.

Zhang, X., Pazner, M. and Duke, N., 2007. Lithologic and mineral information extraction for gold exploration using ASTER data in the South Chocolate Mountains (California). ISPRS J. Photo. and Rem. Sens., 62 (4), 271–282.

Received on: 13-06-2024 ; Revised on: 16-09-2024; Accepted on: 21-09-2024